

## Article

# Selenium Oxoanions Removal from Wastewater by $\text{MoS}_4^{2-}$ Intercalated FeMgAl LDH: Catalytic Roles of Fe and Mechanism Insights

Zhuwei Liao <sup>1,2</sup>, Tianxu He <sup>2,3</sup>, Lerong Shi <sup>2</sup>, Yi Liu <sup>4</sup>, Xinquan Zhou <sup>2,5</sup>, Jia Wang <sup>2</sup> , Wan Li <sup>4</sup>, Yong Zhang <sup>4</sup> , Huabin Wang <sup>4,\*</sup>  and Rui Xu <sup>4,\*</sup>

<sup>1</sup> Urban Construction Engineering Division, Wenhua College, Wuhan 430000, China

<sup>2</sup> Department of Environmental Engineering, School of Environmental Science and Engineering, Huazhong University of Science and Technology, Wuhan 430000, China

<sup>3</sup> Tangshan Environmental Monitoring Center, Tangshan 063000, China

<sup>4</sup> School of Energy and Environment Science, Yunnan Normal University, Kunming 650000, China

<sup>5</sup> School of Chemical Engineering and Pharmacy, Henan University of Science and Technology, Luoyang 471000, China

\* Correspondence: hbwang@ynnu.edu.cn (H.W.); ecowatch\_xr@163.com (R.X.); Tel./Fax: +86-27-8779-2151 (H.W.)

**Abstract:** FeMgAl– $\text{MoS}_4$  LDH was successfully synthesized by a one-pot hydrothermal process followed by ion-exchange methods, and this novel adsorbent was first conducted for aqueous selenium and selenate elimination. The Fe as a component for metal cation layers of LDHs could modulate the layer charge density, leading to more functional groups inserted into layers, and more importantly, this heterogeneous Fe can catalyze the surface reactions between Se(IV) or Se(VI) with S(-II) for oxoanions sequestration. The mechanisms are ion exchange between functional groups with  $\text{HSeO}_3^-$  and  $\text{SeO}_3^{2-}$  for Se(IV) or  $\text{SeO}_4^{2-}$  for Se(VI), followed by reduction by S(-II) from  $\text{MoS}_4^{2-}$  groups. The existence of Fe in LDH cation layers, obviously enhanced the reactions (almost two times more for Se(IV) and three times more for Se(VI), respectively), resulting in satisfying adsorption capacities of 483.9 mg/g and 167.2 mg/g for Se(IV) and Se(VI), respectively. Mechanisms were further revealed by elementary analysis, XRD, FT–IR, SEM–EDX, and XPS, as well as the quantitative study. For sorption kinetics, the calculated values of capacities from the pseudo-second-order model are much closer to the experimental values. For sorption isotherms, Langmuir is better than the Freundlich isotherms model for closer capacities (505 mg/g for selenite and 172 mg/g for selenate). All these results demonstrated that the presence of heterogeneous Fe could catalyze the reduction of Se (IV/VI) for the aqueous system, and maybe other high oxidative states hazardous ions. So FeMgAl– $\text{MoS}_4$  is a kind of novel adsorbent that offers a promising multi-functional and highly efficient solution for water selenium purification.

**Keywords:** FeMgAl– $\text{MoS}_4$  LDH; selenium removal; catalytic roles; surface mechanisms



**Citation:** Liao, Z.; He, T.; Shi, L.; Liu, Y.; Zhou, X.; Wang, J.; Li, W.; Zhang, Y.; Wang, H.; Xu, R. Selenium Oxoanions Removal from Wastewater by  $\text{MoS}_4^{2-}$  Intercalated FeMgAl LDH: Catalytic Roles of Fe and Mechanism Insights. *Catalysts* **2022**, *12*, 1592. <https://doi.org/10.3390/catal12121592>

Academic Editors: Jiangkun Du, Lie Yang and Chengdu Qi

Received: 11 October 2022

Accepted: 28 November 2022

Published: 6 December 2022

**Publisher's Note:** MDPI stays neutral with regard to jurisdictional claims in published maps and institutional affiliations.



**Copyright:** © 2022 by the authors. Licensee MDPI, Basel, Switzerland. This article is an open access article distributed under the terms and conditions of the Creative Commons Attribution (CC BY) license (<https://creativecommons.org/licenses/by/4.0/>).

## 1. Introduction

Selenium is an essential element for both animals and human beings, but with elevated concentrations, this element can be extremely hazardous [1]. There is a confining range between the toxic level and dietary deficiency level (>400  $\mu\text{g}/\text{day}$  and <40  $\mu\text{g}/\text{day}$ , respectively) of selenium ions [2], and exposure to them also may lead to neurological or respiratory problems [3,4]. This chemical and radiologically toxic element has caused many environmental pollution problems worldwide [5], and many countries have conducted strict criteria for selenium control for aqueous systems [6].

To solve these problems, efficient removal approaches of water-borne selenium are very desirable. Biological, chemical, and physical techniques, for instance, bacteria metabolism [7],

microbial cells [8], chemical reduction [9], and adsorption [10] were conducted for the removal of selenium. Among these methods, adsorption is highly attractive due to its economic effectiveness, simple design, and strong sorption functionality [11]. Based on this concept, metal-organic framework [12], titanate nanotube [13], carbon nanotube [14], heterogeneous iron [15,16], magnesium oxide [17], alumina oxide [18], titanium oxide [19], and other metal oxides [20], proved to retard the mobilization of selenium in the environment. However, on the other hand, these materials present limited adsorption capacities for selenium removal (always less than 200 mg/g), much lower than the capacity of other hazardous elements removal, like mercury or lead [21–23]. This phenomenon may be attributed to selenium having a relatively long half-life ( $t_{1/2} \approx 3.27 \times 10^5$  years) and exhibiting stable states in natural conditions [24]. Furthermore, selenium ions exist in the aqueous system as  $\text{HSeO}_3^-$  or  $\text{SeO}_3^{2-}$  for Se(IV), and  $\text{HSeO}_4^-$  or  $\text{SeO}_4^{2-}$  for Se(VI), all of these groups are negatively charged, which further constrains the capacities of many adsorbents for selenium removal [25]. Hence, the synthesis of effective adsorbents for this recalcitrant contaminant is still a challenge.

Layered double hydroxide (LDH) was widely applied for the removal of negatively charged pollutants in an aqueous system. As a common two-dimensional material, LDH consists of hosting layers (positively charged) and electrical balance anion groups in the interlayer space [26]. Various kinds of LDHs, such as MgAl–Cl LDH, ZnAl–Cl LDH, MgFe–CO<sub>3</sub> LDH, and other LDHs were synthesized and applied for the sequestration of Oxoanions [27–29]. Another lamellar structure, layered rare earth hydroxides (LRHs), such as  $\text{Y}_2(\text{OH})_5\text{Cl} \cdot 1.5\text{H}_2\text{O}$ , was also synthesized for selenium oxoanions removal [30], exhibited good selectivity while the capacities were constrained (207 mg/g for selenite and 124 mg/g for selenate), and the removal mechanisms were the formation of inner-sphere complexation (for selenite) or outer-sphere complexation (for selenate). This material represented the good capacities of inorganic adsorbents, but these values were still not satisfied, which indicated more mechanisms may need to be involved if intending to promote adsorption performance. Other interlayer species with more functionalities for adsorbents were also applied. For example, the  $\text{MoS}_4^{2-}$  anions group attracted increasing attention in recent years [31,32], such as CoFe–MoS<sub>4</sub> LDH being applied for mercury uptake from S–Hg mixed flue gas [33], and MnMgAl–MoS<sub>4</sub> LDH being synthesized for heavy metal removal from the aqueous system [34]. Besides that, MgAl–MoS<sub>4</sub> LDH was also conducted for selenium treatment, after the ion exchange between foreign selenium oxoanions with interlayer anions, the following reaction of Se(IV) reduced into Se(0) while S(-II) (existed in  $\text{MoS}_4^{2-}$ ) oxidized into S(VI) (existed as  $\text{SO}_4^{2-}$ ) was observed. However, this MgAl–MoS<sub>4</sub> LDH exhibited a good performance (294 mg/g of selenite), with the presence of extra heavy metals in the solution (like  $\text{Hg}^{2+}$  or  $\text{Cd}^{2+}$ ) only, which could accelerate the selenium capture by enhanced reactions between  $\text{MoS}_4^{2-}$  anions and heavy metal ions, leading to more functional groups being released into the solution [35]. However, it is difficult to find such types of wastewater with different pollutants while adding heavy metals from external sources might bring more second pollution. Due to this consideration, multi-mechanisms and efficient adsorbents for selenite and selenate immobilization without potential environmental risks are still very desirable for applications.

More recently, iron ions were widely conducted for the removal of selenium Oxoanions [36]. On the one hand, Fe was one of the widest distribution elements in the natural system, more notably, Fe was proven to play a crucial catalytic role in selenium removal, with the formation of inner-sphere complexation with selenium oxoanions [37–40], and promising reductive potential with selenite or selenate (especially for  $\text{Fe}^{2+}$ ). Accordingly, iron-contained ores, such as maghemite [41], granite [42], goethite [43], ferrihydrite [44], and hematite [45] were used for investigation of the interface reactions with selenium, adsorption processes or transformation on surfaces. Apart from their coordinating advantages, natural iron ores render lower capacities because of their nonporous structure, which results in metals coordinating on the surface only. To overcome these drawbacks, many porous and highly reductive iron-based adsorbents were synthesized, like nanoscale

zero-valent iron (nZVI) [46], which was an effective material with simultaneous adsorption and reduction for Se, and other nZVI-based systems were also developed, such as nZVI/LDH [47], nZVI/Fe<sub>3</sub>O<sub>4</sub>/Fe(II) [48], but the oxidation-related problems of nZVI systems were big issues [49]. One study by Hong et al. made iron-impregnated food waste biochar to remove Se(VI) from an aqueous solution [21]. Another study by Satyro, S, et al. found that the Fe-biochar composites, which were made by impregnating iron (ferric nitrate) onto regular biochar (RB) and steam-activated biochar can remove Se(VI) [22]. However, these studies are the key to the research about S(-II). It was proved that lamellar LDH arrangement can provide protection surroundings against solubility as well as direct oxygen exposure of Fe(II) as well as S(-II) [50], and our group synthesized Fe-based LDH via the co-precipitation method for heavy metals removal, while iron ions could modulate the basal spacing of resultant adsorbent [51]. Additionally, sulfur is also essential for Se removal (such as S(-II) in MoS<sub>4</sub><sup>2-</sup> anions group) [52], and the knowledge gap still exists for the potential roles of Fe ions as reducing agents or catalysts for the sequestration of selenium with the presence of S(-II) involved functional groups.

In this work, we addressed a suitable adsorbent with a good ability to remove unconventional pollutants. We synthesized MoS<sub>4</sub><sup>2-</sup> intercalated FeMgAl layered double hydroxide (FeMgAl–MoS<sub>4</sub> LDH, abbr. FeMgAl–MoS<sub>4</sub>), and reported that the potential reductive and catalytic abilities of Fe ions were favorable to the removal of selenium oxoanions. Specifically, FeMgAl–MoS<sub>4</sub> was successfully synthesized via hydrothermal reactions coupled with anion-exchange processes and then firstly conducted to selenium oxoanions sequestration in the aqueous system. In addition, selenium oxoanions uptake capabilities of FeMgAl–MoS<sub>4</sub> were also compared with other types of cationic inorganic sorbents and intermediate sorbents for a quantitative study, and the sorption mechanisms and the roles of iron ions were unraveled by the combination of elemental analysis, XPS, SEM–EDX, XRD, FT–IR, and Raman techniques. The results clearly demonstrated that Fe could modulate the charge densities of cationic layers, leading to more functional groups inserted into galleries, after that, leaching functional groups could further catalyze with selenium oxoanions by S(-II) reduction, Fe acted as a catalyst for these reductive reactions, which created advantages in terms of uptake capacities and efficiency for selenium sequestration. The presence of heterogeneous Fe could catalyze the reduction of Se(IV/VI) for the aqueous system, and maybe as well as other high oxidative states hazardous ions.

## 2. Results and Discussion

### 2.1. Characterization

Physical and chemical characterizations of FeMgAl–MoS<sub>4</sub> and FeMgAl–NO<sub>3</sub> were conducted through many techniques, compared with MgAl–NO<sub>3</sub> and MgAl–MoS<sub>4</sub> adsorbents also listed. With the general formula of  $[M^{2+}_{1-x} M^{3+}_x (OH)_2]^{x+} (A^{n-})_{x/n} \cdot mH_2O$ , where M<sup>2+</sup> and M<sup>3+</sup> denote the divalent and trivalent metal cations, A<sup>n-</sup> represents the interlayer anions or groups and x is defined as the molar ratio of M<sup>2+</sup> to (M<sup>2+</sup> + M<sup>3+</sup>), we could calculate the formula of the adsorbent (SI Table S1). Elementary Analysis and ICP were conducted to elucidate the components of these adsorbents, as different adsorbents exhibited different features. There was an obvious difference in nitrogen content between MgAl–NO<sub>3</sub> and MgAl–MoS<sub>4</sub> because NO<sub>3</sub><sup>-</sup> in the solution was exchanged with initial CO<sub>3</sub><sup>2-</sup> groups and stable MgAl–NO<sub>3</sub> was collected for further preparation. MgAl–MoS<sub>4</sub> was obtained via this hydrothermal combined with the anion-exchange method, the value of MoS<sub>4</sub><sup>2-</sup> groups was close to the reference value (0.16 and 0.17, respectively), also placing hydrothermal as a good method for LDH preparation. However, there were more functional groups obtained in the LDH structures when Fe was added as the basic component of LDH layers, this phenomenon attributed to Fe could modulate the charge density of LDH layers, and more MoS<sub>4</sub><sup>2-</sup> groups were needed to balance the charge. Moreover, according to the mass balance and charge balance of final resultants, different partials of Fe(II) and Fe(III) can be calculated. With the initial iron ion Fe(II) from the FeCl<sub>2</sub>·4H<sub>2</sub>O, the Fe in the resultant FeMgAl–MoS<sub>4</sub> adsorbent combined with 74% Fe(III) and 26% Fe(II), these values

are in accordance with the following XPS results, and the states of Fe in the adsorbent will be discussed in the following sections.  $\text{NO}_3^-$  groups remained in  $\text{MgAl-MoS}_4$  and  $\text{FeMgAl-MoS}_4$  adsorbents, which means the anion-exchange process was not complete, and  $\text{CO}_3^{2-}$  groups were also observed, indicating the pollution of  $\text{CO}_2$  from the air was not entirely prevented.

The SEM was applied to evaluate the spacing morphology of the resultant adsorbent. As shown in Figure 1,  $\text{FeMgAl-MoS}_4$  shows the typically layered symmetry of the adsorbent, and these images confirmed the dominant structure in the adsorbent was the hexagonal prismatic shape. Moreover, this plate-layered structure illustrated that the resultant  $\text{FeMgAl-MoS}_4$  remained stable even when shaken in solution for several days for anion-exchange processes, which proved the good stability and potential reusability of this adsorbent.  $\text{FeMgAl-MoS}_4$  was successfully obtained by the hydrothermal process coupled with anion exchange, which placed this fabrication method as an acceptable method for LDH preparation, while consistent nitrogen was purged into the solution during preparation processes.

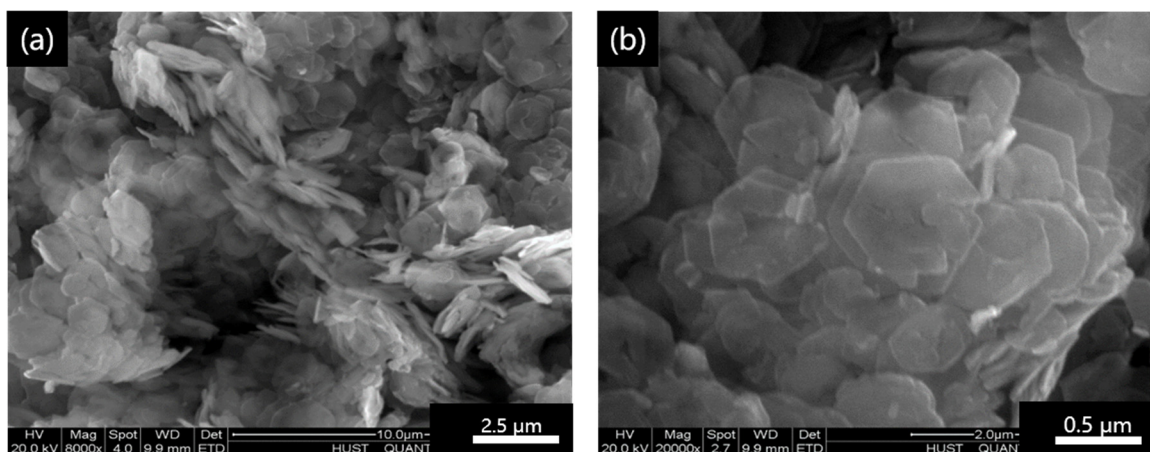


**Figure 1.** Characterization of the microstructure of the  $\text{FeMgAl-MoS}_4$  material. SEM images with magnification factors of 2.5  $\mu\text{m}$  (a), and 0.5  $\mu\text{m}$  (b).

The X-ray diffraction (XRD) further offered detailed distinctions on the crystal structure and basal spacing ( $d_{\text{basal}}$ ) of these obtained adsorbents (SI Figure S2). Diffraction peaks at  $2\theta$  of  $11^\circ$ ,  $21^\circ$ ,  $34^\circ$ ,  $61^\circ$ , and  $62^\circ$  represented that the LDH structure was obviously detected for these adsorbents [53], placing this hydrothermal process and followed anion-exchange accessible for LDH preparation. However, some signals were weak and shifted a little ( $11^\circ$  and  $21^\circ$ ) for  $\text{MgAl-MoS}_4$  and  $\text{FeMgAl-MoS}_4$ , which may be attributed to consistent nitrogen being purged into the solution during the preparation processes, but the LDH structure was still formed and further proved by the SEM observation mentioned before. More importantly, the basal spacing of LDH galleries was different from these LDHs,  $\text{FeMgAl-MoS}_4$  has an enlarged  $d_{\text{basal}}$  (0.96 nm) compared with  $\text{FeMgAl-NO}_3$  (0.83 nm), which rectified the interlayer species of  $\text{MoS}_4^{2-}$ , and the same phenomenon was observed when  $\text{MoS}_4^{2-}$  was introduced into  $\text{MgAl-NO}_3$ , this was in agreement with [51]. Moreover,  $d_{\text{basal}}$  decreased from  $\text{MgAl-MoS}_4$  (1.05 nm) to  $\text{FeMgAl-MoS}_4$  (0.96 nm) when the iron was added as a component for LDH synthesis. The  $d_{\text{basal}}$  of the resultant  $\text{FeMgAl-MoS}_4$  is familiar with  $\text{SeO}_3^{2-}$  intercalated LDHs according to [35] (0.94/0.96 nm for  $\text{SeO}_3^{2-}$  and 0.92 nm for  $\text{SeO}_4^{2-}$ ), which was beneficial to the substitution between selenium oxoanions and inner functional groups via as-prepared  $\text{FeMgAl-MoS}_4$  adsorbent. This hypothesis on suitable  $d_{\text{basal}}$  enhanced the anion exchange processes for  $\text{SeO}_3^{2-}$  and  $\text{SeO}_4^{2-}$  and will be further demonstrated in the following section.

FT-IR spectra were applied to further clarify the changes in the surface functional groups of these adsorbents (SI Figure S3). Wavenumber 3551, 3450, 3440, and 3420  $\text{cm}^{-1}$  of

these adsorbents contributed to the vibration of O–H stretching, which could form complexations with heavy metal cations. While the typical band at  $1587\text{ cm}^{-1}$  in  $\text{MgAl-NO}_3$  ( $1597\text{ cm}^{-1}$  for  $\text{FeMgAl-NO}_3$ ,  $1602\text{ cm}^{-1}$  for  $\text{MgAl-MoS}_4$ , and  $1607\text{ cm}^{-1}$  for  $\text{FeMgAl-MoS}_4$ ) proved the presence of  $\text{CO}_3^{2-}$ , which was consistent with XRD results, that may be attributed to part of the  $\text{CO}_2$  pollution and incomplete anion exchange processes between  $\text{NO}_3^-$  and  $\text{CO}_3^{2-}$ . After the introduction of  $\text{MoS}_4^{2-}$ , a strong band  $1359\text{ cm}^{-1}$  assigned to  $\text{NO}_3^-$  almost disappeared, as the  $1131$  and  $1127\text{ cm}^{-1}$  for M–O confirmed intercalation in the interlayer region of  $\text{MgAl-MoS}_4$  and  $\text{FeMgAl-MoS}_4$ . Moreover, a clear vibration band when the wavenumber was below  $1000\text{ cm}^{-1}$  was associated with the metal–oxygen (M–O) or with metal–sulfur (M–S), which further confirmed the existence of  $\text{MoS}_4^{2-}$  in adsorbents. When adding Fe as a component of adsorbents, there are some shifts with the metal–oxygen (M–O) or with metal–sulfur (M–S) bands, as  $836\text{ cm}^{-1}$  shifted to  $806\text{ cm}^{-1}$ ,  $676\text{ cm}^{-1}$  shifted to  $656\text{ cm}^{-1}$  for  $\text{MgAl-NO}_3$  and  $\text{FeMgAl-NO}_3$  adsorbents, while  $986$ ,  $826$ ,  $690\text{ cm}^{-1}$  for  $\text{MgAl-MoS}_4$  shifted to  $996$ ,  $792$ ,  $666\text{ cm}^{-1}$  for  $\text{FeMgAl-MoS}_4$ , respectively. The  $\delta(\text{O-M-O})$  vibration band showed no changes for different adsorbents at  $438\text{ cm}^{-1}$ . Additionally, M–S stretching and M–O vibration overlapped in the range of  $459\text{--}482\text{ cm}^{-1}$ , and Raman spectra (SI Figure S4) provided evidence to distinguish them. The Mo–S stretching of  $(\text{NH}_4)_2\text{MoS}_4$  was observed at  $479\text{ cm}^{-1}$ , which was in agreement with a reference value ( $300\text{--}515\text{ cm}^{-1}$ ) [54]. In the case of  $\text{FeMgAl-MoS}_4$ , Mo–S stretching appeared at  $287$ ,  $375$ , and  $390\text{ cm}^{-1}$ , this phenomenon could be attributed to a crystal or bridge structure between metal ions and sulfur ions in the LDHs, as  $\text{Mo}(\text{S-M-LDH})$  [55]. These FT–IR results above were also consistent with the aforementioned elementary analysis and proved the presence of related elements or groups.

To sum up, according to Elementary Analysis, XRD, FT–IR, Raman, and SEM, we confirmed the  $\text{FeMgAl-MoS}_4$  was successfully prepared via the hydrothermal method coupled with the anion-exchange process and the presence of heterogeneous Fe could catalyze the reduction of Se (IV/VI) for the aqueous system. Compared with  $\text{MgAl-NO}_3$  or  $\text{FeMgAl-NO}_3$ , we found  $\text{MoS}_4^{2-}$  groups introduced into LDHs and made a series of changes in characteristics. Furthermore, after comparison with  $\text{MgAl-MoS}_4$ , we found  $\text{FeMgAl-MoS}_4$  has more functional groups introduced and a smaller  $d_{\text{basal}}$  for LDH galleries, the same phenomenon was observed when  $\text{MgAl-NO}_3$  opposed to  $\text{FeMgAl-NO}_3$ , more  $\text{NO}_3^-$  groups were introduced and a smaller  $d_{\text{basal}}$  when Fe as a component of metal ions. These distinctions also directly led to their distinguished performance in selenium removal which will be discussed in the following sections.

## 2.2. Adsorption of Selenium

To evaluate the performances of different adsorbents and further disclose the roles of iron ions, a comparison was conducted and experimental values were listed in SI Table S2. Without any adjustments of pH, the pHs of resultant adsorbents are a little higher for Se(IV) than Se(VI), this is may be attributed to the formation of  $\text{HSeO}_3^-$  for the Se(IV) and increased pH values. Based on the previous reports [10], selenium oxoanions form aqueous solutions and are negligible in alkaline surroundings because the surfaces of inorganic oxides are usually negatively charged and therefore repulse anionic selenium species. The selenate species are  $\text{SeO}_4^{2-}$  when  $\text{pH} > 2$ , as for selenite species, the main state is  $\text{HSeO}_3^-$  at  $\text{pH} < 5$ , and  $\text{HSeO}_3^-$  could coexist with  $\text{SeO}_3^{2-}$  at  $\text{pH} 7$  when the pH increased up to 8.5, there are nearly 40%  $\text{HSeO}_3^-$  and nearly 60%  $\text{SeO}_3^{2-}$  in the solution [30]. The removal efficiency of Se(IV) and Se(VI) reached  $484\text{ mg/g}$  and  $167\text{ mg/g}$ , respectively, while the capacities of  $\text{MgAl-NO}_3$  and  $\text{MgAl-MoS}_4$  are  $155\text{ mg/g}$  and  $271\text{ mg/g}$  for Se(IV). The higher capacity achieved compared with  $\text{FeMgAl-NO}_3$  or  $\text{MgAl-NO}_3$  may be due to the reduction process between the introduced selenite or selenate species with inter-layer  $\text{MoS}_4^{2-}$  groups, which will be discussed in the following sections.

### 2.2.1. Quantitative Study

Based on the LDH structure and potential reductive abilities of  $\text{MoS}_4^{2-}$  groups, more details could be elucidated by comparison experiments between LDHs and only  $\text{MoS}_4^{2-}$  groups. Moreover, the hypothetical function of Fe also needs to be investigated, and homogeneous as well as heterogeneous iron ions were conducted for iron performance evaluation, with the results listed in Figure 2, and the calculation processes of ion-exchange or S(-II) reduction utilization percent were demonstrated in SI Table S3. For homogeneous Fe, iron ions came from the proper amount of Fe(II) and Fe(III), adding homogeneous iron ions outside can make a comparison with FeMgAl- $\text{NO}_3$  or FeMgAl- $\text{MoS}_4$ , this Fe as a component of LDH structure, which can be regarded as a heterogeneous Fe resource.

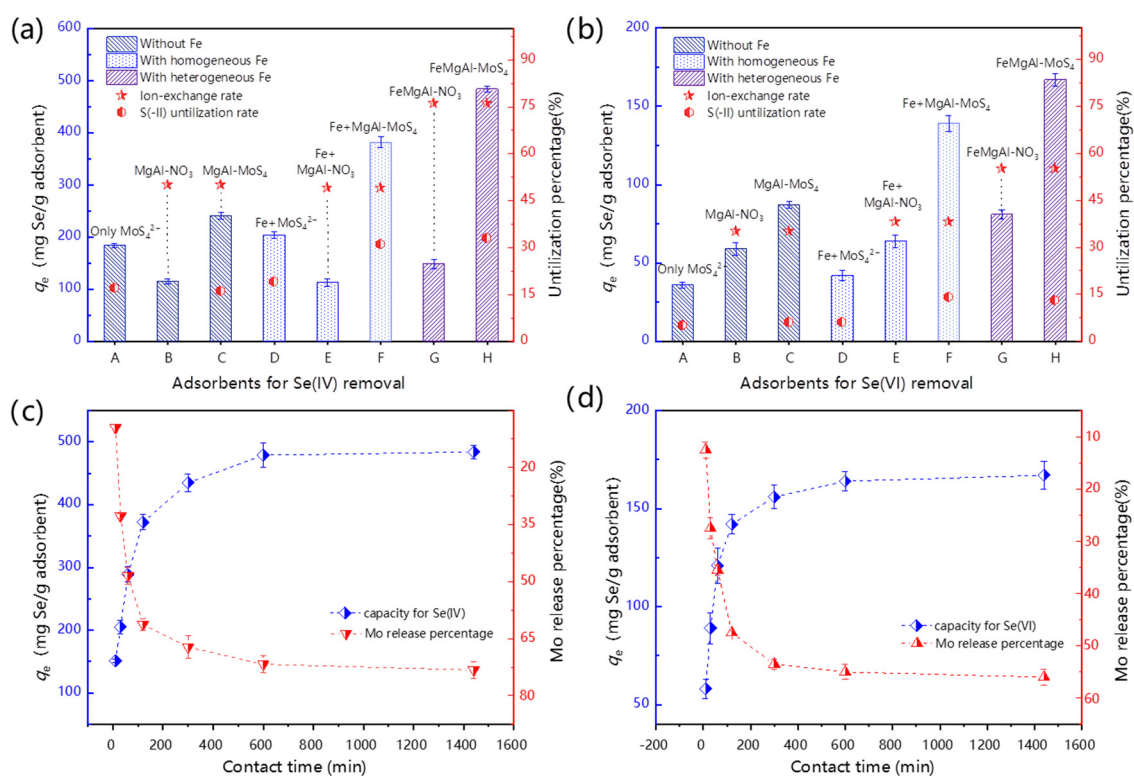


**Figure 2.** Capacities and utilization percent comparison of different adsorbents or their combinations for Se(IV) (a), and Se(VI) (b) removal (Phase ratio = 1.0 g/L, contact time = 24 h, 25 °C,  $C_0(\text{Se}) = 1000$  mg/L, without adjustment of pHs); sorption kinetics and release of Mo ions when Se(IV) (c), and Se(VI) (d) on FeMgAl- $\text{MoS}_4$  (Phase ratio = 1.0 g/L, 25 °C,  $C_0(\text{Se}) = 1000$  mg/L for Se(IV) and 600 mg/L for Se(VI), without adjustment of pHs, at different time intervals).

Individually, for Se(IV) removal, when the solution only contained  $\text{MoS}_4^{2-}$  groups, directly from adding of  $(\text{NH}_4)_2\text{MoS}_4$ , the capacity towards selenium removal is 184 mg/g, according to former research, Mo in the  $\text{MoS}_4^{2-}$  groups could not react with selenium ions [35]. However, based on the charge balance between selenium ions and sulfur ions, one molar S(-II) can reduce two molar Se(IV), with S(-II) oxidized into S(VI) in  $\text{SO}_4^{2-}$  and Se(IV) reduced into Se(0) for removal. Based on this electricity balance, the utilization percentage of S(-II) can be calculated as 16%, and the following S(-II) utilization rates were measured by the same method. Moreover, when MgAl- $\text{NO}_3$  as a comparative LDH adsorbent was applied, the selenite uptake capacity is 115 mg/g, and considering that  $\text{NO}_3^-$  groups are chemically inert, this process presented as an ionexchange process for selenite removal only. Compared with the total amount of anion groups in the LDH layers, the ionexchange rate can be calculated to evaluate the completion degree of the anion groups exchange process between  $\text{HSeO}_3^-$ ,  $\text{SeO}_3^{2-}$ , or  $\text{SeO}_4^-$  with interlayer functional groups. Hence, the ionexchange rate of MgAl- $\text{NO}_3$  was measured as 50%, and this ionexchange rate was also

applied for MgAl–MoS<sub>4</sub> adsorptive reactions, as they both have the same cation layers and close  $d_{\text{basal}}$  values (showed on SI text S1). As mentioned above, MgAl–MoS<sub>4</sub> may combine two functions of ion exchange and follow with S(-II) reduction for selenium removal, the capacity of MgAl–MoS<sub>4</sub> is 271 mg/g, which is close to the reference value (294 mg/g), the lower value of this MgAl–MoS<sub>4</sub> in this experiments may be attributed to the incomplete ion exchange process between CO<sub>3</sub><sup>2-</sup> groups with NO<sub>3</sub><sup>-</sup> groups when in preparation, or attributed to little pollution of CO<sub>2</sub> from the air. According to this data, the ion exchange rate and utilization percentage of MgAl–MoS<sub>4</sub> toward selenite uptake are 50% and 19%, respectively. This 19% is higher than the 17% of directly adding MoS<sub>4</sub><sup>2-</sup> groups, indicating that the LDH structure can protect S(-II) to achieve a higher S(-II) utilization rate and better performance.

Moreover, homogeneous iron ions were added to the solution in order to make a comparison with the heterogeneous Fe of FeMgAl–NO<sub>3</sub> and FeMgAl–MoS<sub>4</sub>. For homogeneous Fe, the adsorption capacity of iron ions was 2 mg/g, which is negligible compared with functions of S(-II) reduction and ion exchange. When combining Fe with only MoS<sub>4</sub><sup>2-</sup> groups, the capacity is 204 mg/g, and S(-II) utilization percentage is 19%, which is better than the 17% of MoS<sub>4</sub><sup>2-</sup> groups alone, suggesting Fe has catalytic ability for S(-II) reductive reactions with Se(IV). Homogeneous Fe alone is inert with Se(IV), also proved by adding iron ions into the MgAl–NO<sub>3</sub> adsorptive process, the capacity is 113 mg/g, and ion-exchange percentage is 49%, even lower than only MgAl–NO<sub>3</sub> (the percentage is 50%), suggesting iron ions are not beneficial to ion exchange, but may be detrimental to this process instead, as iron ions could adhering to the LDH surface could affect Se(IV) adsorption [51]. However, when iron ions are involved with the MgAl–MoS<sub>4</sub> system, the capacity is 382 mg/g, which is much higher than the aforementioned combination of adsorbents and additives. The ion-exchange percentage is the same as MgAl–NO<sub>3</sub> (49%), but the S(-II) utilization percentage is 31%, much higher than this percentage of only MgAl–MoS<sub>4</sub> alone (19%), directly providing evidence that homogeneous iron could catalyze Se(IV) reductive reaction by S(-II), with more details investigated in the following sections. Nevertheless, adding iron ions is complicated for adsorption, and also not realistic for industrial applications as there is less economic efficiency as well as potential environmental risks.

Furthermore, FeMgAl–NO<sub>3</sub> and FeMgAl–MoS<sub>4</sub> were considered as heterogeneous Fe resources, for the consideration of Fe as a component of metal cation layers, and less was soluble in solutions. The performance of these two adsorbents on the sequestration of selenite was also evaluated. In terms of FeMgAl–NO<sub>3</sub>, the capacity is 149 mg/g, as the ion exchange percentage is 76%, which is higher than the MgAl–NO<sub>3</sub> (49%), this may contribute to the Fe as a component of the LDH structure, the resultant adsorbents get more functional groups involved, and the d-space value of Fe-contained LDHs is close to the selenium ions [30], and these are two factors for the ion-exchange process towards the performance improvement of the Fe–contained LDHs. However, for FeMgAl–MoS<sub>4</sub>, the capacity was 484 mg/g, which is the record value for selenium adsorbents described to date, with the ion-exchange percentage of 76% and S(-II) utilization percentage of 33%, which is almost double that of only MoS<sub>4</sub><sup>2-</sup> groups alone (17%), indicating heterogeneous Fe of FeMgAl–MoS<sub>4</sub> exhibits good catalytic performance for Se(IV) reduction by S(-II) ions.

For sequestration of Se(VI), which is regarded as one of the most recalcitrant oxoanions for water purification [36], the same experimental approaches with Se(IV) adsorptive reactions were designed, as the performances were compared to measure the percentages of ion exchange and S(-II) utilization for Se(VI) removal. When the system was no Fe added, the capacities of only MoS<sub>4</sub><sup>2-</sup> groups was 36 mg/g, suggesting the S(-II) utilization percentage was 5%, which was much lower than the value of Se(IV) removal experiment (16%). This may be attributed to the chemically inert Se(VI) in most situations, and this is also the reason why Se(VI) is regarded as one of the most reluctant oxoanions for water purification. Besides that, MgAl–NO<sub>3</sub> was applied to test the ion exchange percentage of the normal layered structure for Se(VI) adsorption. The capacity is 59 mg/g, with an exchange percentage of 35%. Moreover, as a combination of these two functions, MgAl–MoS<sub>4</sub> achieved a

capacity of 87 mg/g, with 35% for ion exchange and 6% for S(-II) reduction. The increase in S(-II) utilization percentage was attributed to the protective layered structure of LDHs, which was in accordance with the phenomenon of Se(IV) removal. Adding iron ions into the solution as the source of homogeneous Fe, the capacities of only  $\text{MoS}_4^{2-}$ ,  $\text{MgAl-NO}_3$ , and  $\text{MgAl-MoS}_4$  systems are 42 mg/g (with 6% sulfur utilization), 64 mg/g (with 38% ion-exchange) and 139 mg/g (with 38% ion-exchange and 14% sulfur utilization), respectively. This increase of S(-II) utilization percentage (from 5% of only  $\text{MoS}_4^{2-}$  groups alone to 14% of  $\text{MoS}_4^{2-}$  adding with Fe), suggests Fe also exhibited good catalytic performance of Se(VI) reduction [56]. In order to further investigations,  $\text{FeMgAl-NO}_3$  and  $\text{FeMgAl-MoS}_4$  were applied as heterogeneous iron sources likewise. The capacities and ion-exchange percentage of  $\text{FeMgAl-NO}_3$  are 81 mg/g and 55%, respectively. Moreover, the ion exchange percentage of 55% for  $\text{FeMgAl-NO}_3$  is higher than this value of  $\text{MgAl-NO}_3$  (35%), indicating the Fe-contained LDHs benefited the Se(VI) adsorption, and the Fe may also be responsible for modulating the LDH cation layer surface charge density, changing the d-space value and involving more functional groups in the adsorbents [18]. Meanwhile, in terms of  $\text{FeMgAl-MoS}_4$ , the capacity reached 167 mg/g, with the contribution of 55% ion-exchange percentage and 13% S(-II) utilization percentage, this capacity is the highest value for Se(VI) by inorganic adsorbents. Besides that, 13% of the S(-II) utilization percentage is almost three times more than the initial  $\text{MoS}_4^{2-}$  groups, demonstrating that heterogeneous Fe could enhance the reactions between Se of(VI) and S(-II).

According to the aforementioned quantitative study, Fe was proven to be an effective catalyst for Se(IV) or Se(VI) reductive reactions with S(-II) from  $\text{MoS}_4^{2-}$  groups, and quantitative amounts were investigated by various experiments, and different contribution rates were also calculated. LDH lamellar structure could protect  $\text{MoS}_4^{2-}$  groups from the pollution of air, and homogeneous iron ions are also benign for selenium reduction, but the performance is not satisfactory. More importantly,  $\text{FeMgAl-MoS}_4$  exhibited valid removal performances both for Se(IV) and Se(VI), for the combination of higher ion-exchange ratios and better efficacy of S(-II) ions from  $\text{MoS}_4^{2-}$  groups, this better efficiency of S(-II) was attributed to the Fe in the  $\text{FeMgAl-MoS}_4$ . The quantitative values and reaction mechanisms were further proved with many techniques such as XPS, XRD, etc., which will be discussed in the following sections.

### 2.2.2. Sorption Kinetics and Isotherms

Sorption kinetics for selenium species removal by  $\text{FeMgAl-MoS}_4$  was investigated to study the reaction rates and sorption pathways. As demonstrated in Figure 2, both Se(IV) and Se(VI), after reaction for 600 min, the concentration deduced to 479 mg/g and 164 mg/g, respectively, the resultant values meeting the aforementioned drinking water standards. The concentrations of Mo ions were also observed by ICP, with the intention of elucidation of ion exchange reactions between  $\text{MoS}_4^{2-}$  groups and  $\text{SeO}_3^{2-}$  or  $\text{SeO}_4^{2-}$  species. The more Mo that existed in the filtrates, the more the selenium species exchanged into LDH layers. If all Mo ions in  $\text{FeMgAl-MoS}_4$  LDH could be leached into solutions, the concentrations of Mo should be 158.4 mg/g adsorbent ( $1/103 \times 0.17 \times 96 \times 1000$ ), but ICP results demonstrated Mo in the solution is 118 mg/g adsorbent, lower than the calculated value, and the ratio is 0.746, which means there were 74.6% Mo ions leaching into solutions. This value was in accordance with the ionexchange utilization percentage of  $\text{FeMgAl-MoS}_4$  (76%), indicating Mo concentrations could represent the leaching of  $\text{MoS}_4^{2-}$  groups, and the lower Mo percentage may be attributed to other functional groups being involved with this ion-exchange process, but the influence was limited. Moreover, the release of Mo ions reached equilibrium at almost 300 min, with a percentage of more than 70%, indicating the equilibrium time of ion exchange is shorter than the equilibrium time of adsorptive reactions. This phenomenon was also observed for Se(VI) removal, which could be attributed to some reactions still existing after ion exchange and this hypothesis was in accordance with the quantitative study, that is S(-II) reduction took place between selenite or selenate ions with exchanged  $\text{MoS}_4^{2-}$  groups, demonstrating there might be two steps

for the reaction: (a) ion-exchange between original functional groups with foreign selenium oxoanions; and (b) leached functional groups reduced other more selenium oxoanions to insoluble states. Two models [57] were applied to the determination of the reaction pathways, which are pseudo-first-order and pseudo-second-order, the sorption rates and other sorption kinetics parameters were used to employ these mechanisms to describe the reaction details and equations are as follows:

pseudo-first-order:

$$\ln(q_e - q_t) = \ln q_e - k_1 t \quad (1)$$

pseudo-second-order:

$$t/q_t = 1/k_2 q_e^2 + (1/q_e)t \quad (2)$$

where  $q_e$  (mg/g) is the amount of target pollutant per unit mass of adsorbent at equilibrium and  $q_t$  (mg/g) is the amount of adsorbed at time  $t$ , while  $k_1$  ( $\text{min}^{-1}$ ) and  $k_2$  ( $\text{g/mg min}^{-1}$ ) are the rate constants when reactions reached equilibrium, both for pseudo-first-order and pseudo-second-order.

Isotherm investigation conducted by adding FeMgAl-MoS<sub>4</sub> as adsorbents into solutions for Se(IV) (SI Table S4) and Se(VI) (SI Table S5) removal and maximum sorption capacities can be calculated. Uptake for the selenium species was increased successively with the Se(IV) and Se(VI) concentrations increased. Sorption of Se(IV) reached an equilibrium when the selenite concentration of 1072 mg/g, and the maximum capacity is 484 mg/g, while Se(VI) reached sorption balance at the concentration of 586 mg/g, and the resultant capacity of Se(VI) is 167 mg/g. The concentrations of element Mo were also observed by the ICP instrument, and pHs before and after reactions were also detected for mechanism understanding. The distribution coefficient  $K_d$  represents the affinity between selenium species and adsorbents, and the  $K_d$  values were summarized and discussed. As known, when  $K_d$  values of >104 mL/g were widely regarded as exceptional adsorbents, and as shown in these tables,  $K_d$  values of these adsorbents are satisfied for applications. The Langmuir isotherms thesis represents the sorption process without mutual interactions between surface sites with adsorbed molecules, and only the monolayer sorption with the homogeneous surface, moreover, all adsorption sites are equivalent to sorption energy. The equation for the Langmuir model [57] was put up as follows:

$$C_e/Q_e = C_e/Q_m + 1/Q_m K_L \quad (3)$$

where  $Q_e$  is the capacity of FeMgAl-MoS<sub>4</sub> towards selenium oxoanions removal (mg/g),  $C_e$  is the equilibrium concentration of selenium oxoanions in solution (mg/L),  $Q_m$  is the maximum capacity of FeMgAl-MoS<sub>4</sub> towards selenium oxoanions (mg/g), while  $K_L$  is the Langmuir coefficient of adsorption on mercury. According to the following equation, related parameters can be calculated and are listed in Table 1. Meanwhile, the Freundlich isotherm model is also widely applied for exponentially decaying adsorption site energy distribution, which is also functional to multilayer adsorption and heterogeneous surface sorption, and the equation of Freundlich isotherms [56] expressed as follows:

$$\log Q_e = \log K_F + 1/n \log C_e \quad (4)$$

where  $K_F$  and  $n$  are the capacity of o and intensity of adsorption, respectively.  $Q_e$  and  $C_e$  are the capacity of FeMgAl-MoS<sub>4</sub> towards selenium oxoanions removal (mg/g) and the initial concentration of selenium oxoanions in an aqueous system (mg/L). Therefore, related parameters can be calculated and listed in Table 1.

**Table 1.** Fitting results of the sorption isotherms and sorption kinetics for selenite and selenate.

Target	Items	Parameter 1	Parameter 2	R <sup>2</sup>
Se(IV)	Adsorption Kinetics			
	Pseudo-first-order	$K_1 = 6.9 \times 10^{-3} \text{ min}^{-1}$	$Q_e = 320.60 \text{ mg g}^{-1}$	0.9111
	Pseudo-second-order	$K_1 = 5.4 \times 10^{-5} \text{ mg/g min}^{-1}$	$Q_e = 500.00 \text{ mg g}^{-1}$	0.9997
	Adsorption isotherm			
	Langmuir	$K_L = 1.8 \times 10^{-3} \text{ L mg}^{-1}$	$Q_m = 505.05 \text{ mg g}^{-1}$	0.9998
	Freundlich	$n = 0.870$	$K_f = 1.38 \text{ mg g}^{-1}$	0.9213
Se(VI)	Adsorption Kinetics			
	Pseudo-first-order	$K_1 = 5.7 \times 10^{-3} \text{ min}^{-1}$	$Q_e = 76.08 \text{ mg g}^{-1}$	0.9436
	Pseudo-second-order	$K_1 = 2.5 \times 10^{-4} \text{ mg/g min}^{-1}$	$Q_e = 169.49 \text{ mg g}^{-1}$	0.9999
	Adsorption isotherm			
	Langmuir	$K_L = 6.1 \times 10^{-3} \text{ L mg}^{-1}$	$Q_m = 172.41 \text{ mg g}^{-1}$	0.9998
	Freundlich	$n = 0.699$	$K_f = 2.38 \text{ mg g}^{-1}$	0.9709

Parameters for fitting sorption kinetics are listed in Table 1. The calculated values of capacities from the pseudo-second-order model are much closer to the experimental values (500 mg/g is close to 484 mg/g for Se(IV), and 170 mg/g is close to 167 mg/g for Se(VI)), and goodness of correlation coefficient (R<sup>2</sup>) is ~1, indicating the selenite and selenate sorption processes by FeMgAl-MoS<sub>4</sub> can be described well by the pseudo-second-order model, which is consistent with a chemisorption process as mentioned above. For sorption isotherms, Langmuir is better than the Freundlich isotherms model for closer capacities (505 mg/g for selenite and 172 mg/g for selenate), indicating the sorption is monolayer sorption and all adsorption sites are equivalent sorption energy. Based on sorption kinetics and isotherms, assumptions of the reaction process could be presented: firstly, selenium oxoanions exchanged with inner MoS<sub>4</sub><sup>2-</sup> groups and related complexation was formed. After that, S(-II) in the released MoS<sub>4</sub><sup>2-</sup> groups could reduce selenite or selenate species, in solutions. Moreover, Fe from the LDH layers was involved as catalysts for selenium reduction for chemical reactions, which will be discussed in the adsorption mechanisms section.

### 2.3. Adsorption Mechanisms

In order to investigate the mechanisms of FeMgAl-MoS<sub>4</sub> for selenium removal, the solid phase after adsorption was dried and analyzed by XRD, FT-IR SEM, and XPS for more details elucidation. After adsorption for different concentrations, the adsorbents maintained the hexagonal prismatic shape, confirming the dominant layered structure even after adsorptive reactions.

XRD patterns and FT-IR spectra of FeMgAl-MoS<sub>4</sub> after adsorption of Se(IV) or Se(VI) are demonstrated in Figure 3. According to a comparison with the original FeMgAl-MoS<sub>4</sub>, peaks at 2θ of 10.0°, 35.6°, and 62.9° could be found, which clearly demonstrate the existence of LDH structure (JCPDS No. 00-039-1346). A new obvious peak at 24.8° of adsorbents formed when Se(IV) concentration was more than 100 ppm, indicating Se(0) was formed, which is consistent with others previously reported on this iron-based compound [35]. When the concentration was low, the main process was ionexchange, and the amount of Se(0) was limited, however, when the selenium concentration was increased, the leached MoS<sub>4</sub><sup>2-</sup> can react with selenium species for further removal process and Se(0) was formed. Moreover, no 30 was observed, indicating no inner-sphere complexation was formed, which is different from other Fe-based materials for selenium immobilization [58], and maybe this was attributed to the states of iron ions on the LDH surface and catalyst roles of Fe, the competition between S(-II) reduction and formation of inner-sphere complexation. The XPS results (Figure 4) also proved there was almost no difference in Fe(II) and Fe(III) percentages before and after adsorption (76% Fe(III) and 24% Fe(II)), and further proved the Fe could act as a catalyst with the same physical and chemical characterizations before and after adsorptive reactions. The same phenomenon was observed for Se(VI) removal, but the Se(0) peaks at 24.8° were too weak to be discernable, indicating the reduction of Se(VI)

is a hard chemical reaction, in accordance with the previous conclusions [50]. However, in the FeMgAl–MoS<sub>4</sub> system, with the presence of Fe, Se(0) was also detected after reactions, calculated by the quantitative study. The  $d_{\text{basal}}$  value is 0.96 nm for used adsorbents, which is much closer to the adsorbents precursor, and for selenite removal, the amount is not large enough to generate a discernible phase, which means FeMgAl–MoS<sub>4</sub> could still act as the dominant phase. When the concentration increased, the  $d_{\text{basal}}$  became more discernible, and the values of  $d_{\text{basal}}$  are nearly no different with other people-prepared SeO<sub>3</sub><sup>2-</sup> LDHs, which suggests the inter-layered anions of materials are almost SeO<sub>4</sub><sup>2-</sup> and SeO<sub>3</sub><sup>2-</sup>. However, a large amount of Mo from ICP analysis of the selenium species adsorbents indicates the existence of MoS<sub>4</sub><sup>2-</sup>, also consistent with the  $d_{\text{basal}}$  of 0.92 nm assigned to SeO<sub>4</sub><sup>2-</sup> LDH. FT-IR spectra confirmed the formation materials and stability of adsorbents after sorption processes, even with the increase in concentrations. After the adsorption, the  $d_{\text{basal}}$  of 0.83 nm of adsorbed FeMgAl–MoS<sub>4</sub> also proved the existence of SO<sub>4</sub><sup>2-</sup> in the structure. The FT-IR band at 1127 cm<sup>-1</sup> in Figure 3 proved the presence of SO<sub>4</sub><sup>2-</sup>, also supported by the XRD data collection revealed the presence of Se(0) [35], which means the degradation of MoS<sub>4</sub><sup>2-</sup> and the reduction process of Se(IV) or Se(VI). For Se(VI), the bands at 996/792 cm<sup>-1</sup> were observed as vibrations of Se–O, which is also found in the salts of Na<sub>2</sub>SeO<sub>4</sub>, which is also in good agreement with the reference data.

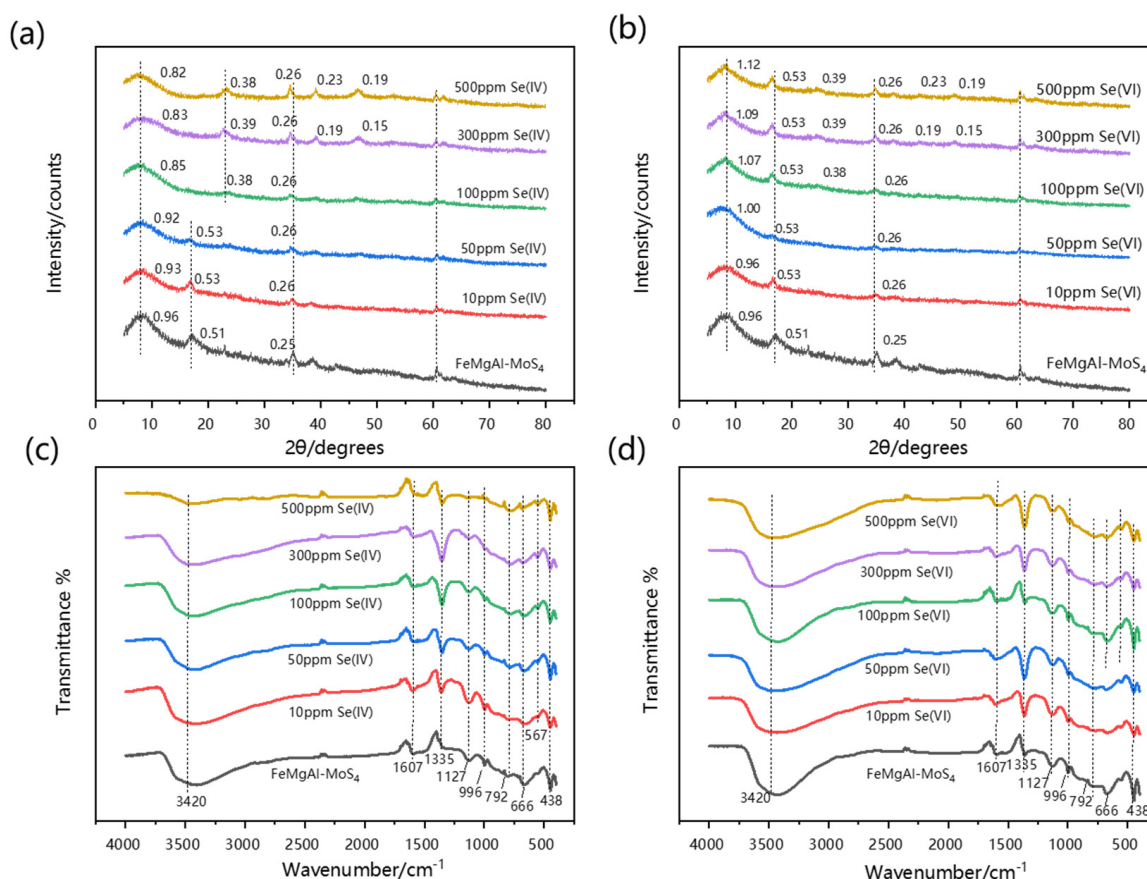


**Figure 3.** XRD patterns of Se(IV) (a), and Se(VI) (b) for different concentrations after adsorption by FeMgAl–MoS<sub>4</sub>; IR spectra of s after FeMgAl–MoS<sub>4</sub> adsorbed Se(IV) (c), and Se(VI) (d) at different concentrations.

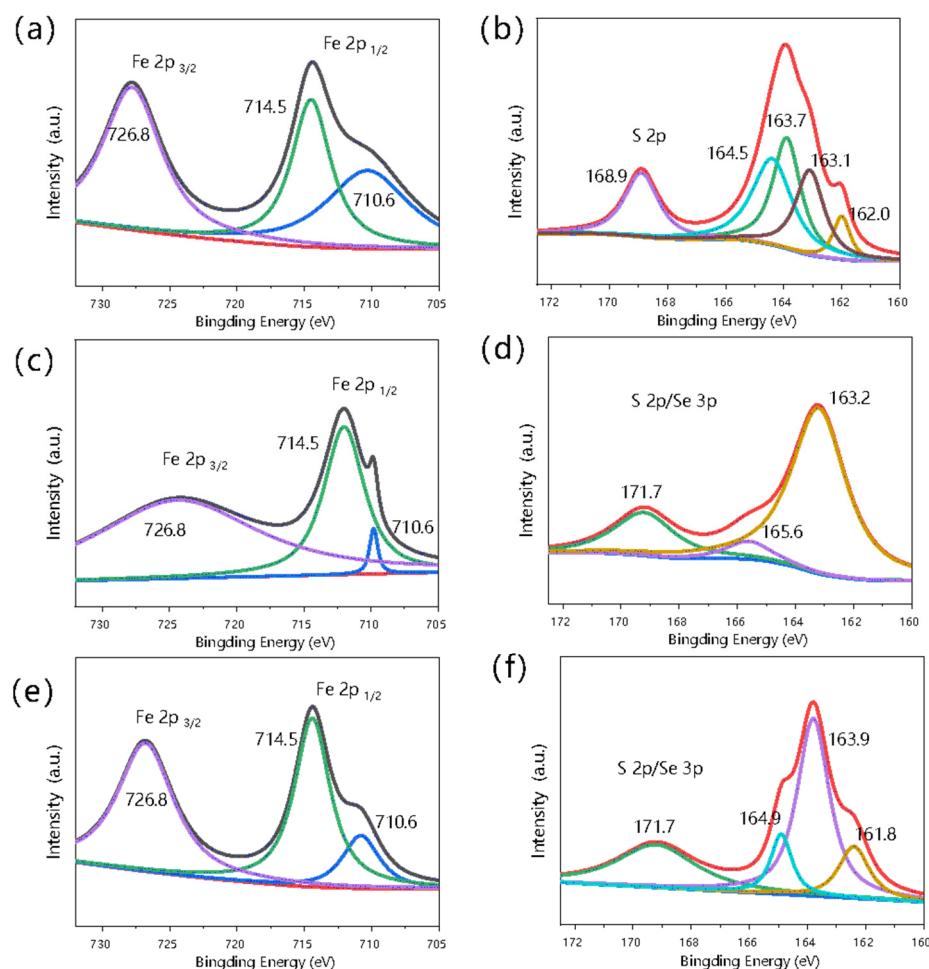


**Figure 4.** X-ray photoelectron spectra with the deconvolution of XPS peaks of Fe2p and S2p/Se3p of original FeMgAl–MoS<sub>4</sub> (a,b), and after FeMgAl–MoS<sub>4</sub> adsorbed 500 ppm Se(IV) (c,d), and 500 ppm of Se(VI) (e,f), respectively.

SEM–EDX (SI Figure S5) also showed Mo uniformly existed on the surface of LDH, further proving some Mo ions remained on the adsorbents after adsorption. The main components of elements on the adsorbed FeMgAl–MoS<sub>4</sub> are Se (28.82 wt%) and S (48.45 wt%), a phenomenon observed both for Se(IV) and Se(VI), demonstrating that when MoS<sub>4</sub><sup>2−</sup> groups are leaching from galleries, the surface reactions are mainly involved with selenite or selenate, as well as S(-II). Mo inserted into LDH galleries is attributed to a similar charge and special structure between MoS<sub>4</sub><sup>2−</sup> and selenium species, as they both have good affinity with LDH cations layers, but remaining Mo on the adsorbents after reactions also demonstrated the ion exchange process was not complete. When the concentration of Se(IV) or Se(VI) increased, the FeMgAl–MoS<sub>4</sub> could keep a good shape, as exhibited in SI Figure S6, indicating this kind of adsorbent is stable in aqueous systems.

XPS was conducted to reveal the detailed changes of these surface elements before and after adsorption. A freshly prepared FeMgAl–MoS<sub>4</sub> Fe(III) is a dominant state of iron ions, and the ratio of Fe(III) (76%) at 714.5 eV and Fe(II) (24%) at 710.6 eV was in agreement with element analysis calculation. Sulfur ions in adsorbed FeMgAl–MoS<sub>4</sub> were detected and XPS peaks at 168–170 eV also support the existence of SO<sub>4</sub><sup>2−</sup>, attributed to the oxidation of S(-II), and consistent with XRD and FT-IR results. For XPS analysis, Se(IV) and Se(VI) as discussed above, the Se 3p energies around 163 eV (Se 3p<sub>1/2</sub>) and 170 eV (Se 3p<sub>3/2</sub>) also verified the capture of selenium, which is also consistent with the reduction of Se(IV), and the reduction of Se(IV) and Se(VI) to Se(0) is mainly accompanied by the oxidation of S(-II) to S(VI), and the relative peak of S 2p energy (~168 eV) was also observed.

As discussed, the mechanism of Se(IV) and Se(VI) oxoanions removal can be demonstrated in two steps for the reaction and exhibited in Figure 5: (a) ion-exchange between original functional groups with foreign selenium oxoanions; and (b) leached functional groups reduced other more selenium oxoanions to insoluble states. With the good affinity between  $\text{MoS}_4^{2-}$  and LDH layers, the ion exchange processes are not complete. The remaining selenium species in the solution could reduce by leached S(-II), and the resultant Se(0) was observed for both Se(IV) and Se(VI) reduction, and  $\text{SO}_4^{2-}$  formed as the oxidative resultant of S(-II), and then as the substitute of  $\text{MoS}_4^{2-}$  inserted into LDH galleries. Moreover, iron species on the FeMgAl-MoS<sub>4</sub> also reacted with Se species to enhance the reductive reactions. All these mechanisms contributed to the record-high removal capacities for selenite and selenate species and were compared with other adsorbents in Table 1.

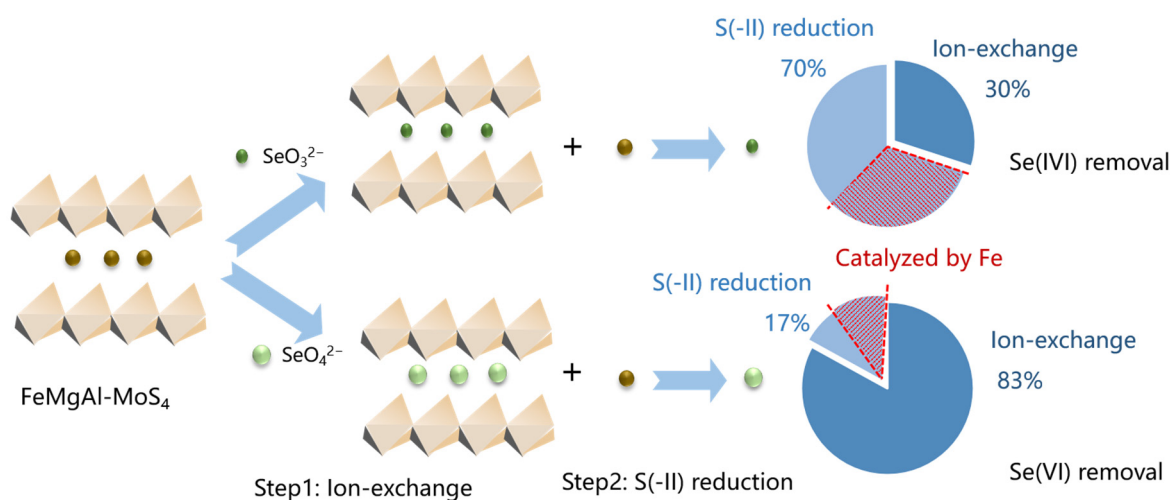


**Figure 5.** Sorption processes and Fe roles towards selenite and selenate removal by FeMgAl-MoS<sub>4</sub>.

### 3. Material and Methods

#### 3.1. Synthesis and Characterization

FeMgAl-MoS<sub>4</sub> was synthesized via a hydrothermal process followed by anion-exchange methods (SI Figure S1). Briefly, 0.3 g FeCl<sub>2</sub>·4H<sub>2</sub>O (1.5 mM), 2.5 g MgCl<sub>2</sub>·6H<sub>2</sub>O (12.5 mM), 1.2 g AlCl<sub>3</sub>·6H<sub>2</sub>O (5 mM) were mixed in 50 mL deionized water, and added to 2.5 g HMT (17.5 mM). All were mixed and a Teflon-lined autoclave was used for the hydrothermal process for 24 h under the temperature of 140 °C. Then CO<sub>3</sub><sup>2-</sup> intercalated FeMgAl layered double hydroxide (FeMgAl-CO<sub>3</sub> LDH, abbr. FeMgAl-CO<sub>3</sub>) was further applied for the synthesis of NO<sub>3</sub><sup>-</sup> intercalated FeMgAl layered double hydroxide (FeMgAl-NO<sub>3</sub> LDH, abbr. FeMgAl-NO<sub>3</sub>). 0.8 g FeMgAl-CO<sub>3</sub> was put into degassed deionized water, nitrogen was purged into the system with the speed of 0.05 L/min through a sealed conical flask, to avoid, or at least minimize the pollution of CO<sub>2</sub> from the air. After that, FeMgAl-MoS<sub>4</sub> LDH was synthesized by simultaneously adding FeMgAl-NO<sub>3</sub> LDH and (NH<sub>4</sub>)<sub>2</sub>MoS<sub>4</sub> into deionized water, ultra-sonication, and washed and vacuum filtrated, dried. The detailed synthesis routes of the different LDHs, including MgAl-CO<sub>3</sub>, MgAl-NO<sub>3</sub>, and MgAl-MoS<sub>4</sub> are described in the Supporting Information (SI).

#### 3.2. Batch Experiments

The sorption experiments for FeMgAl-MoS<sub>4</sub> for the Se(IV) and Se(VI) oxoanions were performed at room temperature (25 °C), Se(IV), and Se(VI) solutions with different concentrations in sealed polytetrafluoroethylene bottles at room temperature, the pH values were generally local values as dissolving related salts to proper concentrations, for the selenium removal were carried out adding 0.01 g of adsorbents to 10 mL of Se(IV) and Se(VI) solutions to achieve mass/volume ratio (m/V) to 1.0 g/L. The uptake experiments were performed by dispersing 0.01 g of FeMgAl-MoS<sub>4</sub> into 10 mL (m/V = 1.0 g/L) of

aqueous solutions in 30 mL polypropylene centrifuge tubes, after blending the prepared solutions with adsorbents, these as-obtained mixtures in the centrifuge tubes were shaken for 24 h, to ensure enough contact between oxoanions and adsorbents. After reaction for 24 h, liquid and solid phases were separated by centrifugation and concentrations of elements through ICP–MS, the capacity of adsorbents was calculated by the equation of  $q_e = (C_0 - C_f) V/m$ , where  $q_e$  is the capacity of adsorbents (mg/g),  $V$  is the solution volume (mL),  $m$  is the mass of adsorbents (mg).  $C_0$  and  $C_f$  are the concentrations of elements before and after reactions, respectively. The distribution coefficient ( $K_d$ ) in adsorption processes is calculated by the equation of  $K_d = (V \times [(C_0 - C_f)/C_f])/m$ , and removal percentage of elements was calculated by  $100\% \times (C_0 - C_f)/C_0$ .

### 3.3. Quantitative Study

For comparison of directly reduced selenium amount with the heterogeneous FeMgAl–MoS<sub>4</sub> reduced amount, homogeneous experiments were conducted by adding 4.3 mg (NH<sub>4</sub>)<sub>2</sub>MoS<sub>4</sub> for 10 mL solution, in order to simulate the same amount of MoS<sub>4</sub><sup>2−</sup> groups in FeMgAl–MoS<sub>4</sub>. For the same reason, the proper amount of iron ions, 0.9 mg FeCl<sub>2</sub>·4H<sub>2</sub>O and 3.42 mg FeCl<sub>3</sub>·6H<sub>2</sub>O to simulate the Fe content and molar ratio of FeMgAl–MoS<sub>4</sub> for each 10 mL solution, 1000 ppm Se(IV) or Se(VI) was used to evaluate maximum adsorptive capacities. Moreover, without Fe experiments were conducted with only (NH<sub>4</sub>)<sub>2</sub>MoS<sub>4</sub>, MgAl–NO<sub>3</sub>, and MgAl–MoS<sub>4</sub> while homogeneous Fe experiments were conducted by using FeCl<sub>2</sub>·4H<sub>2</sub>O and FeCl<sub>3</sub>·6H<sub>2</sub>O as Fe sources instead of Fe-contained LDHs. FeMgAl–NO<sub>3</sub> and FeMgAl–MoS<sub>4</sub> were regarded as heterogeneous Fe sources and used for heterogeneous experiments. XPS is also involved in incomputable experiments with the aim of elucidation of reaction mechanisms.

## 4. Environmental Implications

In the above analysis, we form the conclusion that MoS<sub>4</sub><sup>2−</sup> groups introduced into LDHs made a series of changes in characteristics compared with MgAl–NO<sub>3</sub> or FeMgAl–NO<sub>3</sub>. More importantly, the remaining selenium species in the solution could reduce by leached S(-II), and the resultant Se(0) was observed for both Se(IV) and Se(VI) reduction, and SO<sub>4</sub><sup>2−</sup> formed as the oxidative resultant of S(-II), and then as the substitute of MoS<sub>4</sub><sup>2−</sup> inserted into LDH galleries. Moreover, Fe from the LDH layers was involved as catalysts for selenium reduction for chemical reactions, which will be discussed in the adsorption mechanisms section. With the good affinity between MoS<sub>4</sub><sup>2−</sup> and LDH layers, the ion exchange processes are not complete.

Oxoanions are always regarded as categories of reluctant pollutants in the natural system, negatively charged and chemically inert making them hard to immobilize. Selenium in the environment has raised great concern for its stability and long-term radiotoxicity. Synthetic or natural inorganic mineral materials were widely applied for selenium uptake. However, previous reports mostly focused on investigations of detailed interaction mechanisms more than the improvement of adsorptive capacities. Reduction coupled with adsorption (like the nZVI-related system) is a solution, but economically feasible adsorbents are still desirable. Therefore, a novel Fe-catalyzed system for selenium uptake was designed, the roles of Fe in FeMgAl–MoS<sub>4</sub> were investigated and reaction mechanisms for oxoanions removal were also elucidated. All the results presented in our work confirmed that the FeMgAl–MoS<sub>4</sub> could be a promising and emerging adsorbent for the efficient removal of selenium oxoanions, maybe even other oxoanions environmental pollutants.

**Supplementary Materials:** The following are available online at <https://www.mdpi.com/article/10.3390/catal12121592/s1>. Figure S1: Scheme of adsorbents preparation, Figure S2: XRD patterns, Figure S3: FT-IR spectra, Figure S4: Raman spectra, Figure S5: SEM morphology and EDX profile of LDH, Supplementary Figure S6: SEM images of the original FeMgAl–MoS<sub>4</sub> adsorbents (a) and samples after FeMgAl–MoS<sub>4</sub> adsorbed of (b, b') 10 ppm Se(IV) and 10 ppm Se(VI), (c, c') 100 ppm Se(IV) and Se(VI), (d, d') 200 ppm Se(IV) and Se(VI), (e, e') 500 ppm Se(IV) and Se(VI), Table S1:

Elemental analysis, the chemical formula of synthesized LDH, Table S2: Comparison of selenite and selenate removal capacity, Table S3: Calculated values of maximum uptake capacities ( $q_m$ ) for oxoanions calculated based on ion-exchange or S(-II) reduction or combined, Table S4: Sorption isotherms of Se(IV) on FeMgAl-MoS<sub>4</sub>.

**Author Contributions:** Z.L.: Experiments and manuscript organization. T.H.: Manuscript writing. L.S.: Experiments. Y.L., X.Z. and W.L.: Experiments. Y.Z. and J.W.: Manuscript structure guidance. H.W.: Guidance, review, and editing. R.X.: Guidance, review, and editing. All authors have read and agreed to the published version of the manuscript.

**Funding:** This work was supported by Natural Science Foundation of Hubei Province (ZRMS2021001892), National Natural Science Foundation of China (22264025), Yunnan Plateau Characteristics of Bio-fertilizer (202202AE090025), Applied Basic Research Foundation of Yunnan Province (202201AS070020, 202201AU070061), Yunnan Province Education Department Project (2022J0136), Yunnan Provincial Observation and Research Station (202105AM07003), and Yunnan Academy of Experts Workstation (YSZJGZZ-2021062).

**Conflicts of Interest:** The authors declare that the research was conducted in the absence of any commercial or financial relationships that could be construed as a potential conflict of interest.

## References

1. Holmes, A.B.; Gu, F.X. Emerging nanomaterials for the application of selenium removal for wastewater treatment. *Environ. Sci. Nano* **2016**, *3*, 982–996. [[CrossRef](#)]
2. Ma, B.; Fernandez-Martinez, A.; Grangeon, S.; Tournassat, C.; Findling, N.; Carrero, S.; Tisserand, D.; Bureau, S.; Elkaim, E.; Marini, C.; et al. Selenite Uptake by Ca–Al LDH: A Description of Intercalated Anion Coordination Geometries. *Environ. Sci. Technol.* **2018**, *52*, 1624–1632. [[CrossRef](#)] [[PubMed](#)]
3. Mayordomo, N.; Foerstendorf, H.; Lützenkirchen, J.; Heim, K.; Weiss, S.; Alonso, U.; Missana, T.; Schmeide, K.; Jordan, N. Selenium(IV) Sorption Onto  $\gamma$ -Al<sub>2</sub>O<sub>3</sub>: A Consistent Description of the Surface Speciation by Spectroscopy and Thermodynamic Modeling. *Environ. Sci. Technol.* **2018**, *52*, 581–588. [[CrossRef](#)]
4. Qin, H.-B.; Takeichi, Y.; Nitani, H.; Terada, Y.; Takahashi, Y. Tellurium Distribution and Speciation in Contaminated Soils from Abandoned Mine Tailings: Comparison with Selenium. *Environ. Sci. Technol.* **2017**, *51*, 6027–6035. [[CrossRef](#)]
5. Carrero, S.; Fernandez-Martinez, A.; Pérez-López, R.; Poulain, A.; Salas-Colera, E.; Nieto, J.M. Arsenate and Selenate Scavenging by Basaluminite: Insights into the Reactivity of Aluminum Phases in Acid Mine Drainage. *Environ. Sci. Technol.* **2016**, *51*, 28–37. [[CrossRef](#)]
6. Ilgen, A.G.; Kruichak, J.N.; Artyushkova, K.; Newville, M.G.; Sun, C. Redox Transformations of As and Se at the Surfaces of Natural and Synthetic Ferric Nontronites: Role of Structural and Adsorbed Fe(II). *Environ. Sci. Technol.* **2017**, *51*, 11105–11114. [[CrossRef](#)]
7. Luo, J.-H.; Chen, H.; Hu, S.; Cai, C.; Yuan, Z.; Guo, J. Microbial Selenate Reduction Driven by a Denitrifying Anaerobic Methane Oxidation Biofilm. *Environ. Sci. Technol.* **2018**, *52*, 4006–4012. [[CrossRef](#)]
8. Yu, Q.; Boyanov, M.I.; Liu, J.; Kemner, K.M.; Fein, J.B. Adsorption of Selenite onto *Bacillus subtilis*: The Overlooked Role of Cell Envelope Sulfhydryl Sites in the Microbial Conversion of Se(IV). *Environ. Sci. Technol.* **2018**, *52*, 10400–10407. [[CrossRef](#)] [[PubMed](#)]
9. Yang, Z.; Xu, H.; Shan, C.; Jiang, Z.; Pan, B. Effects of brining on the corrosion of ZVI and its subsequent As(III/V) and Se(IV/VI) removal from water. *Chemosphere* **2017**, *170*, 251–259. [[CrossRef](#)]
10. Zhang, N.; Gang, D.D.; McDonald, L.; Lin, L.-S. Background electrolytes and pH effects on selenate adsorption using iron-impregnated granular activated carbon and surface binding mechanisms. *Chemosphere* **2018**, *195*, 166–174. [[CrossRef](#)]
11. Qin, H.; Sun, Y.; Yang, H.; Fan, P.; Qiao, J.; Guan, X. Unexpected effect of buffer solution on removal of selenite and selenate by zerovalent iron. *Chem. Eng. J.* **2018**, *334*, 296–304. [[CrossRef](#)]
12. Howarth, A.J.; Katz, M.J.; Wang, T.C.; Platero-Prats, A.E.; Chapman, K.W.; Hupp, J.T.; Farha, O.K. High efficiency adsorption and removal of selenate and selenite from water using metal-organic frameworks. *J. Am. Chem. Soc.* **2015**, *137*, 7488–7494. [[CrossRef](#)] [[PubMed](#)]
13. Hu, B.; Chen, G.; Jin, C.; Hu, J.; Huang, C.; Sheng, J.; Sheng, G.; Ma, J.; Huang, Y. Macroscopic and spectroscopic studies of the enhanced scavenging of Cr(VI) and Se(VI) from water by titanate nanotube anchored nanoscale zero-valent iron. *J. Hazard. Mater.* **2017**, *336*, 214–221. [[CrossRef](#)] [[PubMed](#)]
14. Lee, C.-G.; Kim, S.-B. Removal of arsenic and selenium from aqueous solutions using magnetic iron oxide nanoparticle/multi-walled carbon nanotube adsorbents. *Desalination Water Treat.* **2016**, *57*, 28323–28339. [[CrossRef](#)]
15. Xia, X.; Ling, L.; Zhang, W.-X. Solution and surface chemistry of the Se(IV)-Fe(0) reactions: Effect of initial solution pH. *Chemosphere* **2017**, *168*, 1597–1603. [[CrossRef](#)]
16. He, J.; Qiao, X.; Shi, Y.; Li, Y.; Yang, X.; Zhou, W.; Liu, C. Influence of inherent iron and oxygen concentrations on selenite sorption process using bentonite. *Sci. China Ser. B Chem.* **2017**, *60*, 1258–1264. [[CrossRef](#)]

17. Cui, W.; Li, P.; Wang, Z.; Zheng, S.; Zhang, Y. Adsorption study of selenium ions from aqueous solutions using MgO nanosheets synthesized by ultrasonic method. *J. Hazard. Mater.* **2018**, *341*, 268–276. [[CrossRef](#)]
18. Yamani, J.S.; Lounsbury, A.W.; Zimmerman, J.B. Adsorption of selenite and selenate by nanocrystalline aluminum oxide, neat and impregnated in chitosan beads. *Water Res.* **2014**, *50*, 373–381. [[CrossRef](#)]
19. Jordan, N.; Müller, K.; Franzen, C.; Brendler, V. Temperature impact on the sorption of selenium(VI) onto anatase. *J. Colloid Interface Sci.* **2013**, *390*, 170–175. [[CrossRef](#)]
20. Xie, W.; Liang, Q.; Qian, T.; Zhao, D. Immobilization of selenite in soil and groundwater using stabilized Fe–Mn binary oxide nanoparticles. *Water Res.* **2015**, *70*, 485–494. [[CrossRef](#)]
21. Hong, S.-H.; Lyonga, F.N.; Kang, J.-K.; Seo, E.-J.; Lee, C.-G.; Jeong, S.; Hong, S.-G.; Park, S.-J. Synthesis of Fe-impregnated biochar from food waste for Selenium(VI) removal from aqueous solution through adsorption: Process optimization and assessment. *Chemosphere* **2020**, *252*, 126475. [[CrossRef](#)] [[PubMed](#)]
22. Satyro, S.; Li, H.; Dehkoda, A.M.; McMillan, R.; Ellis, N.; Baldwin, S.A. Application of Fe-biochar composites for selenium (Se+6) removal from aqueous solution and effect of the presence of competing anions under environmentally relevant conditions. *J. Environ. Manag.* **2020**, *277*, 111472. [[CrossRef](#)] [[PubMed](#)]
23. Ifthikar, J.; Jiao, X.; Ngambia, A.; Wang, T.; Khan, A.; Jawad, A.; Xue, Q.; Liu, L.; Chen, Z. Facile One-Pot Synthesis of Sustainable Carboxymethyl Chitosan—Sewage Sludge Biochar for Effective Heavy Metal Chelation and Regeneration. *Bioresour. Technol.* **2018**, *262*, 22–31. [[CrossRef](#)] [[PubMed](#)]
24. Fernandez-Martinez, A.; Charlet, L. Selenium environmental cycling and bioavailability: A structural chemist point of view. *Rev. Environ. Sci. Bio/Technol.* **2009**, *8*, 81–110. [[CrossRef](#)]
25. He, Y.; Xiang, Y.; Zhou, Y.; Yang, Y.; Zhang, J.; Huang, H.; Shang, C.; Luo, L.; Gao, J.; Tang, L. Selenium contamination, consequences and remediation techniques in water and soils: A review. *Environ. Res.* **2018**, *164*, 288–301. [[CrossRef](#)]
26. Long, X.; Wang, Z.; Xiao, S.; An, Y.; Yang, S. Transition metal based layered double hydroxides tailored for energy conversion and storage. *Mater. Today* **2016**, *19*, 213–226. [[CrossRef](#)]
27. You, Y.; Vance, G.F.; Zhao, H. Selenium adsorption on Mg–Al and Zn–Al layered double hydroxides. *Appl. Clay Sci.* **2001**, *20*, 13–25. [[CrossRef](#)]
28. Qu, P.; Li, Y.; Huang, H.; Wu, G.; Chen, J.; He, F.; Wang, H.; Gao, B. Foamed urea-formaldehyde microspheres for removal of heavy metals from aqueous solutions. *Chemosphere* **2019**, *241*, 125004. [[CrossRef](#)]
29. He, C.; Lin, H.; Dai, L.; Qiu, R.; Tang, Y.; Wang, Y.; Duan, P.-G.; Ok, Y.S. Waste shrimp shell-derived hydrochar as an emergent material for methyl orange removal in aqueous solutions. *Environ. Int.* **2019**, *134*, 105340. [[CrossRef](#)]
30. Zhu, L.; Zhang, L.; Li, J.; Zhang, D.; Chen, L.; Sheng, D.; Yang, S.; Xiao, C.; Wang, J.; Chai, Z.; et al. Selenium Sequestration in a Cationic Layered Rare Earth Hydroxide: A Combined Batch Experiments and EXAFS Investigation. *Environ. Sci. Technol.* **2017**, *51*, 8606–8615. [[CrossRef](#)]
31. Ma, L.; Wang, Q.; Islam, S.M.; Liu, Y.; Ma, S.; Kanatzidis, M.G. Highly Selective and Efficient Removal of Heavy Metals by Layered Double Hydroxide Intercalated with the  $\text{MoS}_4^{2-}$  Ion. *J. Am. Chem. Soc.* **2016**, *138*, 2858–2866. [[CrossRef](#)] [[PubMed](#)]
32. Ma, L.; Islam, S.M.; Liu, H.; Zhao, J.; Sun, G.; Li, H.; Ma, S.; Kanatzidis, M.G. Selective and Efficient Removal of Toxic Oxoanions of As(III), As(V), and Cr(VI) by Layered Double Hydroxide Intercalated with  $\text{MoS}_4^{2-}$ . *Chem. Mater.* **2017**, *29*, 3274–3284. [[CrossRef](#)]
33. Xu, H.; Yuan, Y.; Liao, Y.; Xie, J.; Qu, Z.; Shangguan, W.; Yan, N.  $[\text{MoS}_4]^{2-}$  Cluster Bridges in Co–Fe Layered Double Hydroxides for Mercury Uptake from S–Hg Mixed Flue Gas. *Environ. Sci. Technol.* **2017**, *51*, 10109–10116. [[CrossRef](#)] [[PubMed](#)]
34. Ali, J.; Wang, H.; Ifthikar, J.; Khan, A.; Wang, T.; Zhan, K.; Shahzad, A.; Chen, Z.; Chen, Z. Efficient, stable and selective adsorption of heavy metals by thio-functionalized layered double hydroxide in diverse types of water. *Chem. Eng. J.* **2018**, *332*, 387–397. [[CrossRef](#)]
35. Ma, L.; Islam, S.M.; Xiao, C.; Zhao, J.; Liu, H.; Yuan, M.; Sun, G.; Li, H.; Ma, S.; Kanatzidis, M.G. Rapid Simultaneous Removal of Toxic Anions  $[\text{HSeO}_3]^-$ ,  $[\text{SeO}_3]^{2-}$ , and  $[\text{SeO}_4]^{2-}$ , and Metals  $\text{Hg}^{2+}$ ,  $\text{Cu}^{2+}$ , and  $\text{Cd}^{2+}$  by  $\text{MoS}_4^{2-}$  Intercalated Layered Double Hydroxide. *J. Am. Chem. Soc.* **2017**, *139*, 12745–12757. [[CrossRef](#)] [[PubMed](#)]
36. Tokunaga, K.; Takahashi, Y. Effective Removal of Selenite and Selenate Ions from Aqueous Solution by Barite. *Environ. Sci. Technol.* **2017**, *51*, 9194–9201. [[CrossRef](#)] [[PubMed](#)]
37. Pan, B.; Xiao, L.; Nie, G.; Pan, B.; Wu, J.; Lv, L.; Zhang, W.; Zheng, S. Adsorptive selenite removal from water using a nano-hydrated ferric oxides (HFOs)/polymer hybrid adsorbent. *J. Environ. Monit.* **2009**, *12*, 305–310. [[CrossRef](#)]
38. Chan, Y.T.; Kuan, W.H.; Chen, T.Y.; Wang, M.K. Adsorption mechanism of selenate and selenite on the binary oxide systems. *Water Res.* **2009**, *43*, 4412–4420. [[CrossRef](#)]
39. Szlachta, M.; Gerda, V.; Chubar, N. Adsorption of arsenite and selenite using an inorganic ion exchanger based on Fe–Mn hydrous oxide. *J. Colloid Interface Sci.* **2012**, *365*, 213–221. [[CrossRef](#)]
40. Sharrad, M.O.M.; Liu, H.; Fan, M. Evaluation of FeOOH performance on selenium reduction. *Sep. Purif. Technol.* **2012**, *84*, 29–34. [[CrossRef](#)]
41. Jordan, N.; Ritter, A.; Scheinost, A.C.; Weiss, S.; Schild, D.; Hübner, R. Selenium(IV) uptake by maghemite ( $\gamma\text{-Fe}_2\text{O}_3$ ). *Environ. Sci. Technol.* **2014**, *48*, 1665–1674. [[CrossRef](#)] [[PubMed](#)]
42. Yang, X.; Ge, X.; He, J.; Wang, C.; Qi, L.; Wang, X.-Y.; Liu, C. Effects of Mineral Compositions on Matrix Diffusion and Sorption of  $^{75}\text{Se}(\text{IV})$  in Granite. *Environ. Sci. Technol.* **2018**, *52*, 1320–1329. [[CrossRef](#)] [[PubMed](#)]

43. Nie, Z.; Finck, N.; Heberling, F.; Pruessmann, T.; Liu, C.; Lützenkirchen, J. Adsorption of Selenium and Strontium on Goethite: EXAFS Study and Surface Complexation Modeling of the Ternary Systems. *Environ. Sci. Technol.* **2017**, *51*, 3751–3758. [[CrossRef](#)] [[PubMed](#)]
44. Francisco, P.C.M.; Sato, T.; Otake, T.; Kasama, T.; Suzuki, S.; Shiwaku, H.; Yaita, T. Mechanisms of Se(IV) Co-precipitation with Ferrihydrite at Acidic and Alkaline Conditions and Its Behavior during Aging. *Environ. Sci. Technol.* **2018**, *52*, 4817–4826. [[CrossRef](#)] [[PubMed](#)]
45. Ma, Z.; Shan, C.; Liang, J.; Tong, M. Efficient adsorption of Selenium(IV) from water by hematite modified magnetic nanoparticles. *Chemosphere* **2018**, *193*, 134–141. [[CrossRef](#)]
46. Qin, H.; Li, J.; Yang, H.; Pan, B.; Zhang, W.; Guan, X. Coupled Effect of Ferrous Ion and Oxygen on the Electron Selectivity of Zerovalent Iron for Selenate Sequestration. *Environ. Sci. Technol.* **2017**, *51*, 5090–5097. [[CrossRef](#)]
47. Hu, B.; Ye, F.; Jin, C.; Ma, X.; Huang, C.; Sheng, G.; Ma, J.; Wang, X.; Huang, Y. The enhancement roles of layered double hydroxide on the reductive immobilization of selenate by nanoscale zero valent iron: Macroscopic and microscopic approaches. *Chemosphere* **2017**, *184*, 408–416. [[CrossRef](#)]
48. Tang, C.; Huang, Y.; Zhang, Z.; Chen, J.; Zeng, H.; Huang, Y.H. Rapid removal of selenate in a zero-valent iron/Fe<sub>3</sub>O<sub>4</sub>/Fe<sup>2+</sup> synergetic system. *Appl. Catal. B Environ.* **2016**, *184*, 320–327. [[CrossRef](#)]
49. Shan, C.; Chen, J.; Yang, Z.; Jia, H.; Guan, X.; Zhang, W.; Pan, B. Enhanced removal of Se(VI) from water via pre-corrosion of zero-valent iron using H<sub>2</sub>O<sub>2</sub>/HCl: Effect of solution chemistry and mechanism investigation. *Water Res.* **2018**, *133*, 173–181. [[CrossRef](#)]
50. Kameda, T.; Kondo, E.; Yoshioka, T. Equilibrium and kinetic studies of Se(vi) removal by Mg–Al layered double hydroxide doped with Fe<sup>2+</sup>. *RSC Adv.* **2014**, *4*, 61817–61822. [[CrossRef](#)]
51. Jawad, A.; Liao, Z.; Zhou, Z.; Khan, A.; Wang, T.; Ifthikar, J.; Shahzad, A.; Chen, Z.; Chen, Z. Fe–MoS<sub>4</sub>: An Effective and Stable LDH-Based Adsorbent for Selective Removal of Heavy Metals. *ACS Appl. Mater. Interfaces* **2017**, *9*, 28451–28463. [[CrossRef](#)] [[PubMed](#)]
52. Yang, Y.; Chen, T.; Sumona, M.; Gupta, B.S.; Sun, Y.; Hu, Z.; Zhan, X. Utilization of iron sulfides for wastewater treatment: A critical review. *Rev. Environ. Sci. Bio/Technol.* **2017**, *16*, 289–308. [[CrossRef](#)]
53. Jawad, A.; Li, Y.; Lu, X.; Chen, Z.; Liu, W.; Yin, G. Controlled leaching with prolonged activity for Co–LDH supported catalyst during treatment of organic dyes using bicarbonate activation of hydrogen peroxide. *J. Hazard. Mater.* **2015**, *289*, 165–173. [[CrossRef](#)] [[PubMed](#)]
54. Zhou, S.; Zeng, H.C. Boxlike Assemblages of Few-Layer MoS<sub>2</sub> Nanosheets with Edge Blockage for High-Efficiency Hydrogenation of CO<sub>2</sub> to Methanol. *ACS Catal.* **2022**, *16*, 9872–9886. [[CrossRef](#)]
55. Ye, X.; Hou, H.; Xin, X.; Hammer, C. M–S (M=Mo, W) cluster compound films on copper surfaces. *Appl. Surf. Sci.* **1995**, *89*, 151–157. [[CrossRef](#)]
56. Wang, H.; Cui, T.; Chen, D.; Luo, Q.; Xu, J.; Sun, R.; Zi, W.; Xu, R.; Liu, Y.; Zhang, Y. Hexavalent chromium elimination from wastewater by integrated micro-electrolysis composites synthesized from red mud and rice straw via a facile one-pot method. *Sci. Rep.* **2022**, *12*, 14242. [[CrossRef](#)]
57. Wang, H.; Duan, R.; Zhou, X.; Wang, J.; Liu, Y.; Xu, R.; Liao, Z. Efficient removal of mercury and chromium from wastewater via biochar fabricated with steel slag: Performance and mechanisms. *Front. Bioeng. Biotechnol.* **2022**, *10*, 961907. [[CrossRef](#)] [[PubMed](#)]
58. Chan, Y.; Liu, Y.; Tzou, Y.; Kuan, W.; Chang, R.; Wang, M. Kinetics and equilibrium adsorption study of selenium oxyanions onto Al/Si and Fe/Si coprecipitates. *Chemosphere* **2018**, *198*, 59–67. [[CrossRef](#)]